



Why Is Water More Reactive Than Hydrogen in Photocatalytic CO₂ Conversion at Higher Pressures? Elucidation by Means of X-Ray Absorption Fine Structure and Gas Chromatography–Mass Spectrometry

Hongwei Zhang and Yasuo Izumi*

Department of Chemistry, Graduate School of Science, Chiba University, Chiba, Japan

OPEN ACCESS

Edited by:

Junguang Tao,
Hebei University of Technology, China

Reviewed by:

Ellen B. Stechel,
Arizona State University, United States
Federica Valentini,
Università di Roma Tor Vergata, Italy

*Correspondence:

Yasuo Izumi
yizumi@faculty.chiba-u.jp

Specialty section:

This article was submitted to
Green and Sustainable Chemistry,
a section of the journal
Frontiers in Chemistry

Received: 03 July 2018

Accepted: 20 August 2018

Published: 27 September 2018

Citation:

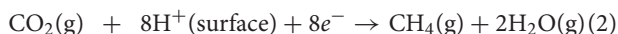
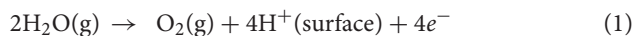
Zhang H and Izumi Y (2018) Why Is Water More Reactive Than Hydrogen in Photocatalytic CO₂ Conversion at Higher Pressures? Elucidation by Means of X-Ray Absorption Fine Structure and Gas Chromatography–Mass Spectrometry. *Front. Chem.* 6:408. doi: 10.3389/fchem.2018.00408

Photocatalytic conversion of CO₂ into mainly methane using Pd/TiO₂ photocatalyst proceeded faster at 0.80 MPa using water rather than hydrogen as a reductant. The former reaction (CO₂ + water) consists of two steps: first, water photosplitting and second, the latter reaction (CO₂ + hydrogen). It was paradoxical that total steps proceeded faster than each step based on simple kinetics. To elucidate the reason, Pd and Ti K-edge X-ray absorption fine structure (XAFS) was monitored during CO₂ photoconversion using H₂ or moisture and the exchange reaction of ¹³CO₂ at Pd/TiO₂ surface was also monitored. As a result, the coordination number, *N*(Ti–O) and *N*[Ti(–O–)Ti] values, decreased from original values for TiO₂ crystalline (6 and 12) to 4.9–5.7 and 9.7–10.6 under CO₂ and moisture, respectively, in contrast to significantly smaller decreases under CO₂ and H₂ and under Ar. The exchange of gas-phase ¹³CO₂ with preadsorbed ¹²CO₂ reached the equilibrium in ~20 h with a rate constant of 0.20 h⁻¹. The reason of the higher activity using water rather than H₂ could be explained owing to the oxygen vacancy (O_v) sites as confirmed by XAFS. The reaction of TiO₂ surface with water formed O_v sites responsible for water oxidation, specially separated from Pd nanoparticle sites for CO₂ reduction. In contrast, Pd nanoparticle sites were competed by CO₂ and H species, and the photoconversion of CO₂ was suppressed at the elevated pressure of CO₂ + H₂.

Keywords: CO₂, oxygen vacancy, X-ray absorption fine structure, gas chromatography–mass spectrometry, ¹³CO₂

INTRODUCTION

Photocatalytic conversion of CO₂ into fuels is one of the routes to producing C neutral fuels without a net increase in atmospheric CO₂ concentrations associated with fossil-derived alternatives (Izumi, 2013). The reaction includes two steps: water oxidation to O₂ followed by CO₂ photoconversion to form methane, etc.



We systematically tested the photocatalytic reaction under CO₂ + H₂ (Table 1A), an essentially identical reaction to Equation (2), for photocatalytic conversion of CO₂ into fuels, if it is combined with the water photo-oxidation step (Equation 1) (Kawamura et al., 2017). Based on the formation rates of C-containing products (CH₄, CO, and methanol) using Pd/TiO₂, water was evidently more reactive (37 μmol-C h⁻¹ g_{cat}⁻¹) than H₂ (8.6 μmol-C h⁻¹ g_{cat}⁻¹) for CO₂ photoconversion at the higher reaction pressures, e.g., 0.80 MPa (Table 1C, G). It was paradoxical that a part of the reaction steps, i.e., Equation (2), was slower than total reaction steps, i.e., Equations (1, 2) based on simple kinetics. In this study, the reason was investigated by X-ray absorption fine structure (XAFS) and gas chromatography–mass spectrometry (GCMS).

MATERIAL AND METHODS

A sample was prepared via liquid phase reduction (Kawamura et al., 2017) from 1.0 mM aqueous solution of Na₂PdCl₄ (>98%, Sigma Aldrich) and TiO₂ (P25, Degussa; anatase: rutile phase = 4:1, specific surface area 60 m² g⁻¹) stirred at 290 K for 24 h. Then, 40 mM of NaBH₄ aqueous solution was added in a molar ratio of Pd: NaBH₄ = 1:8, and the suspension was washed with deionized water (<0.055 μS cm⁻¹) supplied by an RFU424TA system (Advantec) before drying under vacuum at 290 K for 1 h and then filtered. The obtained precipitate was washed with deionized water before drying under vacuum at 290 K for 24 h. The obtained sample was denoted as Pd/TiO₂ and the Pd content was 0.5 weight-% as metal.

For comparison, TiO₂ was also synthesized in the laboratory. Acid solution (1.2 mL of 5 weight-% H₂SO₄ aqueous solution) and 1.37 mL of TiCl₄ were added into 96 mL of deionized water at 273 K under argon atmosphere and stirred at 900 rotations per minute for 30 min. Then, 28 weight-% ammonia aqueous solution was dropped into the solution at 368 K to adjust the pH 7.0. The solution was stirred at the temperature for 1 h and cooled to 290 K. The obtained suspension was filtered and washed by deionized water (total 500 mL) until no chlorine ions were detected using silver nitrate. The thus-obtained powder was dried at 373 K overnight, calcined at 573 K for 2 h, and white TiO₂ powder was obtained. The Pd was loaded on the homemade TiO₂ in a similar manner to the liquid phase reduction for P25 as described earlier.

The high-pressure photoconversion tests were performed in homemade stainless steel reactor equipped with quartz windows (Kawamura et al., 2017; Zhang et al., 2017). A mixed CO₂/H₂ gas or CO₂ gas/moisture was introduced into the reactor. A film (10 mg of photocatalyst) in the reactor was irradiated by a 500-W xenon arc lamp (Model OPM2-502, Ushio) for 5 h. The reaction gas was analyzed using packed columns of 13X-S molecular sieves and polyethylene glycol (PEG-6000) supported on Flusin P (GL Sciences, Inc.) set in a gas chromatograph

equipped with a thermal conductivity detector (GC-TCD; Model GC-8A, Shimadzu).

The Pd K-edge XAFS spectra were measured at 290 K in the transmission mode in the Photon Factory Advanced Ring at the High Energy Accelerator Research Organization (KEK) on beamline NW10A. An Si (3 1 1) double-crystal monochromator and a Pt-coated focusing cylindrical mirror were inserted into the X-ray beam path. A Piezo transducer was used to detune the X-ray intensity to two-thirds of the maximum to suppress higher harmonics (Izumi et al., 2001; Fujishima et al., 2015). The Pd K-edge absorption energy was calibrated to 24348 eV using the spectrum of a Pd metal foil (Bearden, 1967).

The Ti K-edge XAFS spectra were measured in the transmission mode in the Photon Factory at KEK on beamline 9A, 9C, and 12C. An Si(1 1 1) double-crystal monochromator and a pair of bent conical/cylinder mirrors and/or double flat mirrors were inserted into the X-ray beam path. A Piezo transducer was used to detune to two-thirds of the maximum X-ray intensity to suppress higher harmonics (Izumi et al., 2001; Fujishima et al., 2015). Spectra for the Pd/TiO₂ sample (10 mg) diluted by boron nitride were measured under CO₂ (100 kPa) and moisture (2.2 kPa), under CO₂ (70 kPa) and H₂ (30 kPa), or Ar (100 kPa) in the presence/absence of UV-visible light irradiation provided by a 500-W Xe arc lamp (the flux intensity 81.6 mW cm⁻²) at the beamline (Izumi et al., 2007; Morikawa et al., 2014). The Ti K-edge absorption energy was calibrated to 4964.5 eV using the spectrum of a Ti metal foil (Bearden, 1967). The obtained Pd and Ti K-edge XAFS data were analyzed using XDAP software package using modified Victoreen function, spline function, Fourier transform, and multiple-shell curve fitting (Vaarkamp et al., 2006; Izumi et al., 2009).

Isotope-labeled exchange reaction tests were performed and monitored with GCMS using a JMS-Q1050GC (JEOL) apparatus equipped with a quadruple mass spectrometer. Helium (purity > 99.9999%) was used as the carrier gas. The sampling loop comprised a Pyrex glass system vacuumed using rotary and diffusion pumps (10⁻⁶ Pa) and connected to the JMS-Q1050GC using 1.5 m of deactivated fused silica tube (No. 160-2845-10, Agilent; internal diameter 250 μm) maintained at 393 K during the analysis to avoid gas adsorption (Wein et al., 2018).

A photocatalyst sample (0.100 g) was placed in a quartz photoreactor and evacuated at 295 K for 2 h while being connected to a Pyrex glass circulating system (circulating section 206.1 mL) and rotary and diffusion pumps (10⁻⁶ Pa). Then, ¹³CO₂ (0.68 kPa; ¹³C 99%, ¹⁷O 0.1%, ¹⁸O 0.7%, chemical purity > 99.9%, Cambridge Isotope Laboratories, Inc.) photoexchange with the photocatalyst surface was monitored at 295 K under irradiation by UV-visible light from a 500 W xenon arc lamp (Model SX-UID502XAM, Ushio). The distance between the exit of the lamp window and the photocatalyst was 18 mm. The exchange with adsorbed ¹²CO₂ at the surface was monitored using a packed column of PEG-6000 supported on a Flusin P (GL Sciences Inc.) set in the JSM-Q1050GC.

The exchange reaction rates were assumed to follow first-order equilibrium kinetics and the rate constants k_r and k_r' are for the exchange of gas-phase ¹³CO₂ with adsorbed ¹²CO₂ and

TABLE 1 | Results of photocatalytic tests of CO₂ photoconversion for 5 h Using 10 mg of Pd (0.5 weight-%)/TiO₂ Photocatalysts^a and TiO₂ (P25) at 0.12–0.80 MPa.

Entry	Catalyst	Reactants			Formation rates ($\mu\text{mol h}^{-1} \text{g}_{\text{cat}}^{-1}$)				References
		(MPa)		(kPa)	CO	CH ₃ OH	CH ₄	$\Sigma(\text{C-products})^{\text{b}}$	
		CO ₂	H ₂	H ₂ O					
A	Pd/TiO ₂	0.12	0.28		<0.08	<0.004	38	38	Kawamura et al., 2017
a'					<0.08	0.034	5.2	5.3	This work
B	TiO ₂				<0.08	0.027	4.0	4.0	Kawamura et al., 2017
C	Pd/TiO ₂	0.24	0.56		<0.08	<0.004	8.6	8.6	Kawamura et al., 2017
D		0.12		2.3	<0.08	0.065	14	14	Zhang et al., 2017
E		0.40			4.1	0.063	19	23	Zhang et al., 2017
F	TiO ₂				<0.08	<0.004	<0.12	<0.20	Zhang et al., 2017
G	Pd/TiO ₂	0.80			6.3	0.52	30	37	Zhang et al., 2017

^aPrepared using P25 TiO₂ except for entry a' (homemade TiO₂).

^bTotal formation rates for C-containing products.

gas-phase ¹²CO₂ with adsorbed ¹³CO₂, respectively.

$$\frac{dP_{13}\text{CO}_2}{dt} = -k_r P_{13}\text{CO}_2 + k_r' P_{12}\text{CO}_2 \quad (3)$$

$$P_{12}\text{CO}_2 = \frac{k_r}{k_r + k_r'} \left\{ 1 - e^{-(k_r + k_r')t} \right\} P_{13}\text{CO}_2(\text{initial}) \quad (4)$$

$$P_{12}\text{CO}_2(\text{equilibrium}) = \frac{k_r}{k_r + k_r'} P_{13}\text{CO}_2(\text{initial}) \quad (5)$$

$$\therefore P_{12}\text{CO}_2 = P_{12}\text{CO}_2(\text{equilibrium}) \left\{ 1 - e^{-(k_r + k_r')t} \right\} \quad (6)$$

Photocatalytic tests using ¹³CO₂ (2.3 kPa) and H₂ (21.7 kPa) were also performed in a similar apparatus and conditions to that of ¹³CO₂ exchange tests.

RESULTS AND DISCUSSION

Photoconversion Tests of CO₂

First, reported kinetic results are summarized. Both the reactions under CO₂ + H₂ and under CO₂ + moisture critically depended on the pressure of reactants using Pd/TiO₂ (Kawamura et al., 2017; Zhang et al., 2017). The formation rates of C-containing products under CO₂ + H₂ reached a local maximum at 0.40 MPa (0.12 MPa of CO₂, 0.28 MPa of H₂) and drew a volcanolike dependence (Table 1A, C). In Kawamura et al. (2017), the volcanolike local maximum seems distributed relatively steep based on 13 test data points. Methane was a dominant product under the conditions. In contrast, the formation rates followed a typical Langmuir-type dependence, i.e., they gradually increased as a function of reactants pressure under CO₂ + moisture at 0.12–0.80 MPa (Table 1D, E, G) (Zhang et al., 2017). Minor CO and methanol were also produced under the conditions.

Due to the balance of different pressure dependencies between the two types of reactions, H₂ was more reactive at lower than 0.40 MPa, whereas water was more reactive at higher than 0.40 MPa as a reductant for CO₂. In this context, the major question of this study is the reason for the different pressure dependencies of CO₂ photoconversion rates using H₂ vs. water.

Photoconversion test was performed at 0.40 MPa of CO₂ and H₂ using Pd/TiO₂ with the help of homemade TiO₂ (Table 1a'). Methane was the major product similar to the result using Pd/TiO₂ prepared from commercial P25 (Table 1A) (Kawamura et al., 2017). The reason for the difference of the methane formation rates (5.2 $\mu\text{mol h}^{-1} \text{g}_{\text{cat}}^{-1}$ vs. 38 $\mu\text{mol h}^{-1} \text{g}_{\text{cat}}^{-1}$) is not clear, but the crystalline phase (anatase vs. the mixture of anatase and rutile phases) and specific surface area were different. Although the impurity effects for photocatalysts using P25 were suggested (Izumi, 2013; Cybula et al., 2015; Li et al., 2016; Dilla et al., 2017; Grigioni et al., 2017) photoconversion of CO₂ into methane was confirmed using Pd/TiO₂ prepared by not making use of any organic reagents throughout the synthesis procedure of the photocatalyst (Table 1a'). For this problem, several black tests were reported using Pd/TiO₂ (P25), especially the one under UV-visible light and H₂ excluding CO₂ gas (Zhang et al., 2017). No C-containing products were detected above the detection limit of GC-TCD. Thus, a direct impurity effect is denied as the reason for the rate difference (Table 1A, a'). The indirect effect of gas-phase CO₂ on impurity on/in catalyst, leading to the formation of C-containing products under light cannot be denied as the reason for formation rate difference.

The other possibility of formation rate difference is critical pressure dependence of TiO₂-based photocatalysts under CO₂ + H₂ (Kawamura et al., 2017). Due to the critical difference of reactant pressure for the conversion rate maximum (volcano top) for each catalyst, formation rate difference of by a factor of 7.2 times between Pd/TiO₂ (P25) and Pd/TiO₂ (homemade) may result at a fixed reactant pressure (0.40 MPa).

Active Site Monitoring by XAFS

For the morphological characterization of the photocatalysts, transmission electron microscope images for the Pd/TiO₂ catalyst, fresh and used one, after photocatalytic test in CO₂ + H₂ and cross-sectional scanning electron microscope (SEM) images for fresh Pd/TiO₂ were reported in Kawamura et al. (2017). The morphology of the catalyst negligibly changed after the photocatalytic test, but the mean Pd particle size slightly

increased starting from 3.1 to 3.9 nm after the photocatalytic test (Kawamura et al., 2017). Cross-sectional SEM images for fresh Pd/TiO₂ and used one after photocatalytic test in CO₂ + moisture were also reported in Zhang et al. (2017). The color of the top few micrometers of Pd/TiO₂ catalyst film (total 11–16 μm) changed after the photocatalytic test (Zhang et al., 2017). In this study, monitoring of local active sites was performed in addition to these morphological studies.

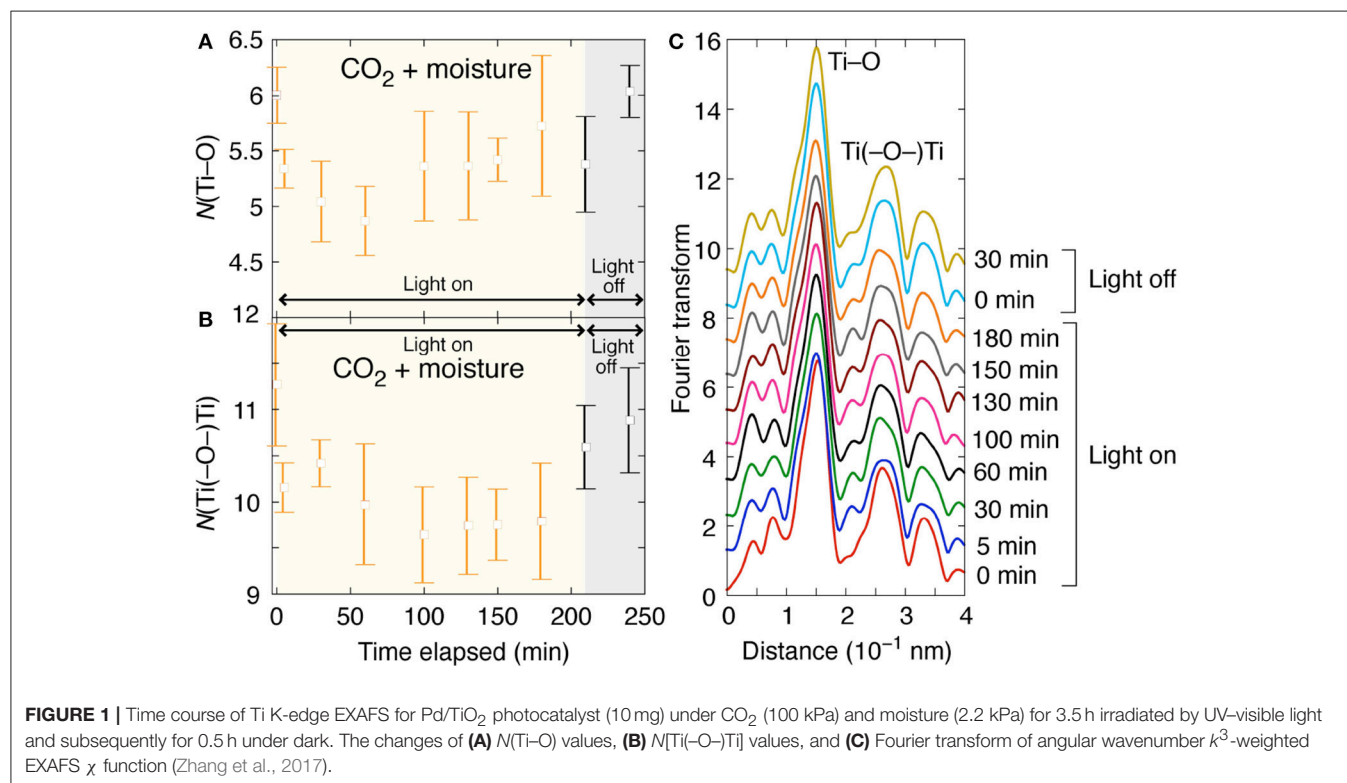
The X-ray absorption near-edge structure (XANES) at the Pd K-edge suggested metallic Pd nanoparticles dispersed on TiO₂. The extended X-ray absorption fine structure (EXAFS) also did not show significant change during photoreactions under CO₂ + H₂ or CO₂ + moisture based on the Pd–Pd shell, but the coordination number $N(\text{Pd}-\text{O})$ decreased from 1.9 for fresh sample to 0.6–0.9 after the photocatalytic tests under CO₂ + H₂ at 0.024–0.40 MPa (Kawamura et al., 2017) and to 0.8–1.0 under CO₂ + moisture at 4.6 kPa–0.40 MPa (Zhang et al., 2017). The decrease of $N(\text{Pd}-\text{O})$ values suggested the formation of oxygen vacancy (O_v) sites on/in TiO₂ near Pd nanoparticles under the reaction conditions of CO₂ photoconversion.

The Ti K-edge XAFS was also investigated under the reaction conditions of CO₂ photoconversion with moisture (Figure 1). Under CO₂ (100 kPa), moisture (2.2 kPa), and UV–visible light, the change in $N(\text{Ti}-\text{O})$ values was monitored (Figure 1A). The changes under light and then under dark were depicted as the Fourier transform in Figure 1C. The intensity of peak for Ti–O interatomic pair at 0.15 nm (phase shift uncorrected) decreased when the light was on (Figure 1C, 5 min), remained almost constant during the light irradiation, and increased to

the original when the light was off (Figure 1C, Light off, 0 min). In accordance with the peak intensity change, in comparison with the initial $N(\text{Ti}-\text{O})$ value (6.0) under CO₂, moisture, and dark, the value significantly decreased to 4.9–5.7 during light irradiation for 3.5 h. At 0.5 h after the light was off, the $N(\text{Ti}-\text{O})$ value increased to the original value (6.0).

The peak intensity of Ti(–O)–Ti interatomic pair at 0.26 nm (phase shift uncorrected; Figure 1C) and the $N[\text{Ti}(\text{O})-\text{Ti}]$ values followed a similar trend: decrease from the initial 11.3 to 9.7–10.6 during the irradiation of UV–visible light (Figure 1B). Taking the experimental and fit errors into account (Figures 1A,B), the $N(\text{Ti}-\text{O})$ and $N[\text{Ti}(\text{O})-\text{Ti}]$ values would evaluate the concentration of O_v sites in/on TiO₂ (Zhang et al., 2017).

Two control monitoring tests were also performed: (i) using H₂ instead of moisture as reductant for CO₂ and (ii) using only argon. First, under CO₂ (70 kPa), H₂ (30 kPa), and UV–visible light, the changes in peak intensity of Ti–O and Ti(–O)–Ti interatomic pair at 0.15 nm and 0.26 nm (phase shift uncorrected), respectively (Figure 2E) and the resultant $N(\text{Ti}-\text{O})$ and $N[\text{Ti}(\text{O})-\text{Ti}]$ values were monitored (Figures 2A,B). The peak intensity of Ti–O interatomic pair decreased at 75 min of light irradiation, but no clear correlation between light irradiation and the Ti–O peak intensity was found. The peak intensity of Ti(–O)–Ti interatomic pair did not change much. In accordance with the peak intensity changes, in comparison with the initial value (5.9) under CO₂, H₂, and dark, the $N(\text{Ti}-\text{O})$ value varied, but within a small range of 5.6–5.8 during light irradiation for 125 min. At 50 min after the light was



off, the $N(\text{Ti-O})$ value increased to the original value (6.0). In comparison with the monitoring under CO₂ and moisture (starting from 6.0 to 4.9–5.7; **Figure 1A**), the decrease in $N(\text{Ti-O})$ value was effectively smaller under CO₂ and H₂ ($\Delta = 0.1$ – 0.3) during photoirradiation. The $N[\text{Ti}(-\text{O})\text{Ti}]$ value remained between 12 and 11.7 under the irradiation of UV–visible light and negligibly changed after the light was off: 12–11.2 (**Figure 2B**). Under CO₂ and moisture, the decrease was greater: from 11.3 to 9.7–10.6 by the effect of light (**Figure 1B**).

Under Ar (100 kPa) and UV–visible light, the $N(\text{Ti-O})$ value changed between 5.7 and 6.0 during light irradiation for 100 min. At 5 min after the light was off, the $N(\text{Ti-O})$ value remained at 5.9 (**Figure 2C**). The changes in $N[\text{Ti}(-\text{O})\text{Ti}]$ values were also minimal under Ar: 12–11 throughout the monitoring test under light/dark (**Figure 2D**). These differences in $N(\text{Ti-O})$ and $N[\text{Ti}(-\text{O})\text{Ti}]$ values were because more O_v sites were formed under the photoreduction of CO₂ using moisture rather than H₂ or Ar.

Monitoring of ¹³CO₂ Exchange by GCMS

The ¹³CO₂ exchange reaction test was performed using Pd–TiO₂ (P25) photocatalyst. The amount of ¹³CO₂ gas gradually decreased over 20 h by the exchange with ¹²CO₂ on Pd–TiO₂ sample that was preadsorbed from air (**Figure 3A**). The changes followed equilibrium kinetics as listed in Equations (3–6), and the formation of ¹²CO₂ (n : mol) in gas phase was well fitted by Equation (6') (**Figure 3A**).

$$n_{12\text{CO}_2}(\mu\text{mol}) = 0.657 + 1.80(1 - e^{-0.20t}) \quad (6')$$

Initial 0.657 μmol is the impurity (1.18 mol%) included in the introduced ¹³CO₂ gas (0.68 kPa). The $n_{12\text{CO}_2}(\text{equilibrium})$ value (1.80 μmol) obtained by the fit of Equation (6') to the data

corresponds to 0.18 molecules of CO₂ adsorbed per nm² of Pd–TiO₂ that was an acceptable value after the evacuation at 295 K for 2 h as pretreatment. The sum of rate constants k_r and k_r' corresponds to total rate constant (Equation 6) to reach the equilibrium ¹³CO₂ and ¹²CO₂ (0.20 h⁻¹).

As a comparison, if we assume that the dispersion of mean 3.1 nm Pd nanoparticles (0.50 weight-%) over TiO₂ observed by transmission electron microscopy (Kawamura et al., 2017) is ~50% (Kip et al., 1987) and the conversion to C-containing products (methane, CO, and methanol) proceeded on the surface of the Pd atoms starting from CO₂, the formation rate of C-containing products (37 μmol h⁻¹ g_{cat}⁻¹) under 0.80 MPa of CO₂ and moisture (**Table 1G**) corresponds to the turnover frequency (TOF)

$$\frac{37 \times 10^{-6} \text{ mol h}^{-1} \text{ g}_{\text{cat}}^{-1} \times 10^{-2} \text{ g}_{\text{cat}}}{\frac{10^{-2} \text{ g}_{\text{cat}} \times 0.005 \times 0.5}{106.42 \text{ g}_{\text{Pd}} \text{ mol}^{-1}}} = 1.6 \text{ h}^{-1}.$$

This comparison is contradictory because the early adsorption equilibrium of CO₂ (0.20 h⁻¹ based on Equation 6') is slower than CO₂ photoreduction to methane via much more difficult reaction steps (1.6 h⁻¹). However, the exchange rate (0.20 h⁻¹) observed under ¹³CO₂ (initial 0.68 kPa) in this study was by a couple of times higher compared with the formation rate of C-containing products under initial 3.4 kPa of CO₂ + 1.2 kPa of moisture (0.9 μmol h⁻¹ g_{cat}⁻¹) (Zhang et al., 2017) corresponding to the TOF

$$\frac{0.9 \times 10^{-6} \text{ mol h}^{-1} \text{ g}_{\text{cat}}^{-1} \times 10^{-2} \text{ g}_{\text{cat}}}{\frac{10^{-2} \text{ g}_{\text{cat}} \times 0.005 \times 0.5}{106.42 \text{ g}_{\text{Pd}} \text{ mol}^{-1}}} = 0.04 \text{ h}^{-1}.$$

The CO₂ exchange was reported using isotope labeled Ti¹⁸O₂ irradiated by XeCl excimer laser (308 nm) to form C¹⁸O₂ and ¹⁶OC¹⁸O (Civiš et al., 2011).

Furthermore, stability test of photocatalytic reaction using ¹³CO₂ (2.3 kPa) + H₂ (21.7 kPa) and Pd/TiO₂ was performed for more than 50 h (**Figure 3B**). To avoid the possibility of

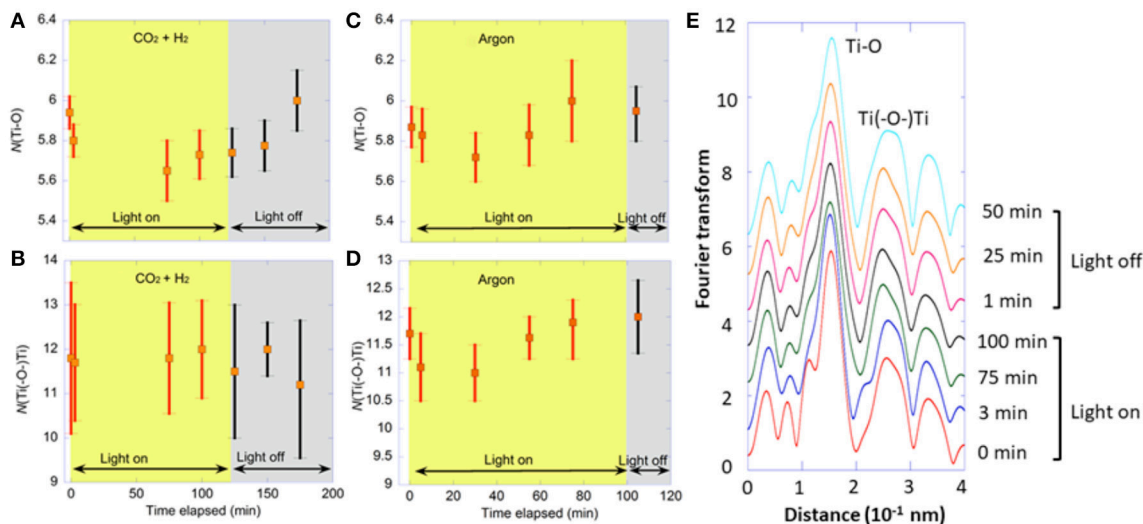
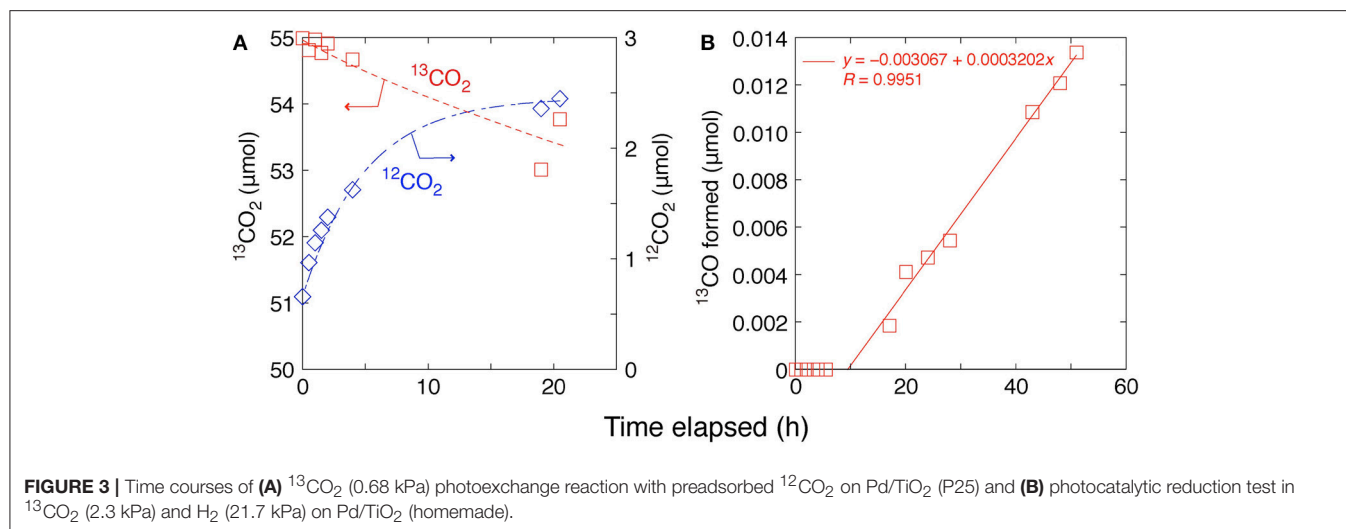


FIGURE 2 | Time course of Ti K-edge (**A–D**) EXAFS for Pd/TiO₂ photocatalyst (10 mg). (**A,B**) Under CO₂ (70 kPa) and H₂ (30 kPa) for 125 min irradiated by UV–visible light and subsequently for 75 min under dark. (**C,D**) Under Ar (100 kPa) for 100 min irradiated by UV–visible light and subsequently for 20 min under dark. The changes of (**A,C**) $N(\text{Ti-O})$ values and (**B,D**) $N[\text{Ti}(-\text{O})\text{Ti}]$ values. (**E**) Fourier transform of angular wavenumber k^3 -weighted EXAFS χ function under CO₂ (70 kPa) and H₂ (30 kPa).



impurity effects, Pd/TiO₂ (homemade) was used and a byproduct ¹³CO was monitored by GCMS rather than methane that may be produced from impurity in TiO₂ (Izumi, 2013; Cybula et al., 2015; Li et al., 2016; Dilla et al., 2017; Grigioni et al., 2017). In accordance with the rate of ¹³CO₂ exchange reaction (Figure 3A), ¹³CO started to be formed at ~10 h of reaction and constantly formed for more than 50 h (Figure 3B). As a byproduct, the formation rate was low 0.0032 μmol h⁻¹ g_{cat}⁻¹ corresponding to the TOF 0.00014 h⁻¹. Nevertheless, the stability test confirmed the availability of Pd/TiO₂ photocatalyst for more than 50 h of photoreaction test.

Thus, we should be careful in the isotope tracing tests as ¹²CO₂ could be included derived from preadsorbed ¹²CO₂ in the reactant ¹³CO₂ and ¹²C-products could be included by the photocatalytic conversion.

The Pd/TiO₂ catalyst used in this study is advantageous for CO₂ photoconversion irradiated by visible light (Kawamura et al., 2017; Zhang et al., 2017). The photocatalytic performance was compared with TiO₂ (P25) in 0.40 MPa of CO₂ + H₂ (Table 1A, B) or CO₂ + moisture (Table 1E, F). The formation rates of total C-containing products were 11% and <0.9% using TiO₂ in comparison with corresponding values using Pd/TiO₂, respectively. As TiO₂ is mostly activated by UV light based on the band gap value (3.2 and 3.0 eV for anatase and rutile phases, respectively) (Izumi, 2013), the increased photoactivity using Pd/TiO₂ could be the effects of localized surface plasmon resonance of Pd nanoparticles owing to visible light irradiation (Kawamura et al., 2017; Zhang et al., 2017).

Thus, the answer to the question as to why water was more reactive than H₂ in photocatalytic CO₂ conversion at higher pressures is that water forms hydroxy radical under the irradiation of UV-visible light (Equation 7) and then O_v sites are formed (Equation 8), but not by using H₂ or Ar. The exchange of CO₂ (Figure 3A) and/or the elimination of C-O bond to form CO are also suggested over O_v sites of Au-Cu-TiO₂ (Neatu et al., 2014), MgO-Pt-TiO₂ (Xie et al., 2014), TiO₂ (Liu et al., 2012, 2016; Li et al., 2017), and theoretical models of defective anatase

(Ji and Luo, 2016), anatase (1 0 1), and small TiO₂ cluster (Lee and Kanai, 2012).



The reactions 7 and 8 proceeded as water oxidation over TiO₂ spatially separated from CO₂ reduction sites on Pd for Equation (2). Thus, the effective redox reaction of Equations (1, 2) proceeded using water. Both the reactions 1 and 2 would proceed competitively on Pd under CO₂ + H₂, and the efficiency followed a volcano-like dependence as a function of partial pressures of reactants (Table 1A, B) (Kawamura et al., 2017).

CONCLUSIONS

The formation of O_v sites was monitored by means of Ti K-edge EXAFS using Pd/TiO₂. The coordination number around Ti atoms clearly demonstrated the effective formation of O_v sites under CO₂, moisture, and UV-visible light in contrast to the much smaller population of O_v sites under CO₂, H₂, and UV-visible light. This difference explained the effective red-ox site separation for water oxidation via ·OH radicals and O_v sites and CO₂ reduction over Pd nanoparticle sites under CO₂, moisture, and UV-visible light. The exchange of ¹³CO₂ with preadsorbed ¹²CO₂ over Pd/TiO₂ reached the equilibrium in ~20 h. This result suggested the earlier step of CO₂ photoconversion, but we need to be aware that ¹²C-products are formed via photocatalytic reaction tests under ¹³CO₂.

AUTHOR CONTRIBUTIONS

This study was planned by YI, most of the experiments and analyses were performed by HZ, and this manuscript was written together.

ACKNOWLEDGMENTS

The authors are grateful for the financial supports from the Grant-in-Aid for Scientific Research C (17K05961, 26410204) from the Japan Society for the Promotion of Science and Leading

Research Promotion Program (2015–) from the Institute for Global Prominent Research, Chiba University. X-ray absorption experiments were conducted under the approval of the Photon Factory Proposal Review Committee (2016G577, 2015G586, 2014G631).

REFERENCES

- Bearden, J. A. (1967). X-ray wavelengths. *Rev. Mod. Phys.* 39, 78–124. doi: 10.1103/RevModPhys.39.78
- Civiš, S., Ferus, M., Kubát, P., Zúkalová, M., and Kavan, L. (2011). Oxygen-isotope exchange between CO₂ and solid Ti¹⁸O₂. *J. Phys. Chem. C* 115, 11156–11162. doi: 10.1021/jp201935e
- Cybula, A., Klein, M., and Zaleska, A. (2015). Methane formation over TiO₂-based photocatalysts: reaction pathways. *Appl. Catal. B* 164, 433–442. doi: 10.1016/j.apcatb.2014.09.038
- Dilla, M., Schlögl, R., and Strunk, J. (2017). Photocatalytic CO₂ reduction under continuous flow high-purity conditions: quantitative evaluation of CH₄ formation in the steady state. *Chem. Cat. Chem.* 9, 696–704. doi: 10.1002/cctc.201601218
- Fujishima, Y., Okamoto, S., Yoshida, M., Itoi, T., Kawamura, S., Yoshida, Y., et al. (2015). Photofuel cell comprising titanium oxide and bismuth oxychloride (BiO_{1-x}Cl_{1-y}) photocatalysts that uses acidic water as a fuel. *J. Mater. Chem. A* 3, 8389–8404. doi: 10.1039/C4TA06824F
- Grigioni, I., Dozzi, M. V., Bernareggi, M., Chiarello, G. L., and Selli, E. (2017). Photocatalytic CO₂ reduction vs. H₂ production: the effects of surface carbon-containing impurities on the performance of TiO₂-based photocatalysts. *Catal. Today* 281, 214–220. doi: 10.1016/j.cattod.2016.05.040
- Izumi, Y. (2013). Recent advances in the photocatalytic conversion of carbon dioxide to fuels with water and/or hydrogen using solar energy and beyond. *Coord. Chem. Rev.* 257, 171–186. doi: 10.1016/j.ccr.2012.04.018
- Izumi, Y., Itoi, T., Peng, S., Oka, K., and Shibata, Y. (2009). Site structure and photocatalytic role of sulfur or nitrogen-doped titanium oxide with uniform mesopores under visible light. *J. Phys. Chem. C* 113, 6706–6718. doi: 10.1021/jp810817y
- Izumi, Y., Kiyotaki, F., Nagamori, H., and Minato, T. (2001). Site-selective XAFS spectroscopy tuned to surface active sites of copper catalysts. *J. Electro. Spectrosc. Relat. Phenomen.* 119, 193–199. doi: 10.1016/S0368-2048(01)00292-4
- Izumi, Y., Konishi, K., Obaid, D. M., Miyajima, T., and Yoshitake, H. (2007). X-Ray absorption fine structure combined with X-ray fluorescence spectroscopy. monitoring of vanadium sites in mesoporous titania, excited under visible light by selective detection of vanadium Kβ_{5,2} fluorescence. *Anal. Chem.* 79, 6933–6940. doi: 10.1021/ac070427p
- Ji, Y., and Luo, Y. (2016). New mechanism for photocatalytic reduction of CO₂ on the anatase TiO₂(1 0 1) surface: the essential role of oxygen vacancy. *J. Am. Chem. Soc.* 138, 15896–15902. doi: 10.1021/jacs.6b05695
- Kawamura, S., Zhang, H., Tamba, M., Kojima, T., Miyano, M., Yoshida, Y., et al. (2017). Efficient volcano-type dependence of photocatalytic CO₂ conversion into methane using hydrogen at reaction pressures up to 0.80 MPa. *J. Catal.* 345, 39–52. doi: 10.1016/j.jcat.2016.10.024
- Kip, B. J., Duijvenvoorden, F. B. M., Koningsberger, D. C., and Prins, R. (1987). Determination of metal particle size of highly dispersed Rh, Ir, and Pt catalysts by hydrogen chemisorption and EXAFS. *J. Catal.* 105, 26–38. doi: 10.1016/0021-9517(87)90005-4
- Lee, D., and Kanai, Y. (2012). Role of four-fold coordinated titanium and quantum confinement in CO₂ reduction at titania surface. *J. Am. Chem. Soc.* 134, 20266–20269. doi: 10.1021/ja309871m
- Li, J., Zhang, M., Guan, Z., Li, Q., He, C., and Yang, J. (2017). Synergistic effect of surface and bulk single-electron-trapped oxygen vacancy of TiO₂ in the photocatalytic reduction of CO₂. *Appl. Catal. B* 206, 300–307. doi: 10.1016/j.apcatb.2017.01.025
- Li, K., Peng, B., and Peng, T. (2016). Recent advances in heterogeneous photocatalytic CO₂ conversion to solar fuels. *ACS Catal.* 6, 7485–7527. doi: 10.1021/acscatal.6b02089
- Liu, L., Jiang, Y., Zhao, H., Chen, J., Cheng, J., Yang, K., et al. (2016). Engineering coexposed {0 0 1} and {1 0 1} facets in oxygen-deficient TiO₂ nanocrystals for enhanced CO₂ photoreduction under visible light. *ACS Catal.* 6, 1097–1108. doi: 10.1021/acscatal.5b02098
- Liu, L., Zhao, H., Andino, J. M., and Li, Y. (2012). Photoalytic CO₂ reduction with H₂O on TiO₂ nanocrystals: comparison of anatase, rutile, and brookite polymorphs and exploration of surface chemistry. *ACS Catal.* 2, 1817–1828. doi: 10.1021/cs300273q
- Morikawa, M., Ahmed, N., Yoshida, Y., and Izumi, Y. (2014). Photoconversion of carbon dioxide in zinc–copper–gallium layered double hydroxides: the kinetics to hydrogen carbonate and further to CO/methanol. *Appl. Catal. B* 144, 561–569. doi: 10.1016/j.apcatb.2013.07.065
- Neatu, S., Maciá-Agulló, J. A., Concepción, P., and Garcia, H. (2014). Gold–copper nanoalloys supported on TiO₂ as photocatalysts for CO₂ reduction by water. *J. Am. Chem. Soc.* 136, 15969–15976. doi: 10.1021/ja506433k
- Vaarkamp, M., Linders, H., and Koningsberger, D. (2006). *XDAP Version 2.2.7, XAFS Services International*. Woudenberg.
- Wein, L. A., Zhang, H., Urushidate, K., Miyano, M., and Izumi, Y. (2018). Optimized photoreduction of CO₂ exclusively into methanol utilizing liberated reaction space in layered double hydroxides comprising zinc, copper, and gallium. *Appl. Surf. Sci.* 447, 687–696. doi: 10.1016/j.apsusc.2018.04.046
- Xie, S., Wang, Y., Zhang, Q., Deng, W., and Wang, Y. (2014). MgO- and Pt-promoted TiO₂ as an efficient photocatalyst for the preferential reduction of carbon dioxide in the presence of water. *ACS Catal.* 4, 3644–3653. doi: 10.1021/cs500648p
- Zhang, H., Kawamura, S., Tamba, M., Kojima, T., Yoshida, M., and Izumi, Y. (2017). Is water more reactive than H₂ in photocatalytic CO₂ conversion into fuels using semiconductor catalysts under high reaction pressures? *J. Catal.* 352, 452–465. doi: 10.1016/j.jcat.2017.06.016

Conflict of Interest Statement: The authors declare that the research was conducted in the absence of any commercial or financial relationships that could be construed as a potential conflict of interest.

Copyright © 2018 Zhang and Izumi. This is an open-access article distributed under the terms of the Creative Commons Attribution License (CC BY). The use, distribution or reproduction in other forums is permitted, provided the original author(s) and the copyright owner(s) are credited and that the original publication in this journal is cited, in accordance with accepted academic practice. No use, distribution or reproduction is permitted which does not comply with these terms.